Controlling wrinkles on the surface of a dielectric elastomer balloon

Guoyong Mao [a,b,c], Xiaoqiang Huang [a,b,c], Mazen Diab [a,b,c,d,*], Junjie Liu [a,b,c], Shaoxing Qu [a,b,c,**]

[a] *State Key Laboratory of Fluid Power & Mechatronic System, Zhejiang University, Hangzhou 310027, China*
[b] *Key Laboratory of Soft Machines and Smart Devices of Zhejiang Province, Zhejiang University, Hangzhou 310027, China*
[c] *Department of Engineering Mechanics, Zhejiang University, Hangzhou 310027, China*
[d] *School of Engineering, Brown University, Providence RI 02912, USA*

ARTICLE INFO

ABSTRACT

When a dielectric elastomer membrane is pre-stretched, inflated and then electromechanically activated, wrinkles may nucleate and propagate. Nucleation site, critical voltage and type of wrinkles can be tuned by controlling the initial pre-stretch, initial inflation pressure and applied voltage. We conduct a hybrid experimental and analytical study to investigate the role of these various parameters on the nucleation and propagation of wrinkles on the surface of an inflated dielectric elastomer balloon. Our results show that pre-stretching the membrane before inflation affects considerably types of wrinkles and their nucleation sites. While wrinkles are more spread throughout the surface of a slightly pre-stretched membrane, they are localized either near the clamped edge or the apex of the inflated balloon with initial large pre-stretch. We also discuss and analyze snap-through instability and electrical breakdown of the activated membrane. A three-dimensional phase diagram that delineates the different operation conditions of the activated dielectric elastomer membrane is constructed to aid designing soft actuators.

© 2016 Elsevier Ltd. All rights reserved.

1. Introduction

For the past two decades, dielectric elastomer (DE), a class of electroactive polymers, has emerged as a promising, low cost smart material that can lend itself to a wide range of applications. This is primarily due to its capability to undergo large voltage-induced deformation. It has been shown, for instance, that a pre-stretched DE membrane may strain beyond 100% [1], and when mounted on a pressurized chamber then electrically stimulated, it may stretch up to 1692% area strain [2]. This behavior coupled with other properties such as high energy density, fast response, quiet operation, and light weight have made DE a viable material to applications such as flexible electronics, sensors, robotics, adaptive optics and energy harvesters [1–5]. Gaining a solid understanding of the instabilities of DE and controlling them as needed are to successfully utilize DE as the smart material it can be.

When a DE membrane is stimulated using an electric field, compressive Maxwell stresses develop in the normal direction to the surface causing in plane stretching of the membrane and significant thinning. Typically, a DE membrane undergoing large deformation may experience three types of failure: mechanical, electrical and pull-in instability. It may also undergo electromechanical

* Corresponding author at: School of Engineering, Brown University, Providence RI 02912, USA.
** Corresponding author at: Department of Engineering Mechanics, Zhejiang University, Hangzhou 310027, China.
E-mail addresses: mazendiab@gmail.com (M. Diab), squ@zju.edu.cn (S. Qu).

phase transition. This electromechanically-induced large deformation needs to be studied and understood in order to control and tailor it to suit the end application. For example, while it is desirable to limit the deformation of DE membrane when used as insulator and capacitor, harnessing this large deformation is essential when used in artificial muscles and energy harvesters [6,7].

While instabilities of DE subject to voltage sometimes lead to failure of the dielectric, it has been recently discovered that the same instabilities, when properly controlled, can produce novel functions such as achieving giant actuation strains [6,7], dynamic surface patterning [8], and active control of biofouling [9]. Wang et al. showed that a curved polymer bonded to a metal base and immersed may develop controllable wrinkles, creases or craters [8]. Mao et al. have recently demonstrated that under a combination of mechanical loading and voltage, an inflated DE membrane may wrinkle [10]. They showed that with suitable coupling of the mechanical and electrical stimuli, locations and patterns of wrinkles may be controlled.

Herein, we investigate wrinkling instability of a pre-stretched DE membrane subject to a combination of internal pressure and voltage with focus on the role of the initial pre-stretch. We adopt the analytical model for the inflated DE membrane as derived in Mao et al. [10] and analyze the wrinkling instability of the DE balloon as a function of pre-stretch, initial inflation pressure and applied voltage. We then create a bifurcation diagram that delineates flat state, snap-through instability and wrinkle instability of the activated DE membrane. The plan of this paper is as follows. In Section 2, the experiment is described and experimental results are presented. In Section 3, a parametric study is conducted to determine the critical conditions for the nucleation of wrinkles and their nucleation sites on the surface of the inflated DE membrane. Also, analytical results are compared with the experimental results in Section 3. A discussion of the electrical breakdown of the DE membrane is presented and the three-dimensional phase diagram is provided in Section 4. Finally, concluding remarks are given in Section 5.

2. Experiment

Fig. 1 illustrates the setup of the experiment. Two kinds of DE membrane acquired from 3M company, VHB 9473 and VHB 4905 with original thickness $H_1 = 0.25$ mm and $H_2 = 0.5$ mm respectively, are coated with carbon grease and then mounted on an air chamber with a fixed radius $R_c = 45$ mm and height $H_c = 200$ mm. The chamber is connected through a check valve to an air pump to inflate the DE membrane. The internal pressure is regulated by a manometer (AZ Instrument Corporation) in the range 0–33.45 kPa, with resolution 0.02 kPa, and accuracy 0.3% of full scale at 25 °C. Upon inflation, voltage is applied to the DE balloon using a step-voltage device with maximum voltage $\phi_{\max} = 10$ kV. The radius of the un-deformed membrane, R_0, is varied where the ratio R_c/R_0 defines the pre-stretch ratio, λ_{pre}, of the DE membrane. Different pre-stretch ratios before air inflation are considered. The initial inflation pressure is varied in the range 50–400 Pa for
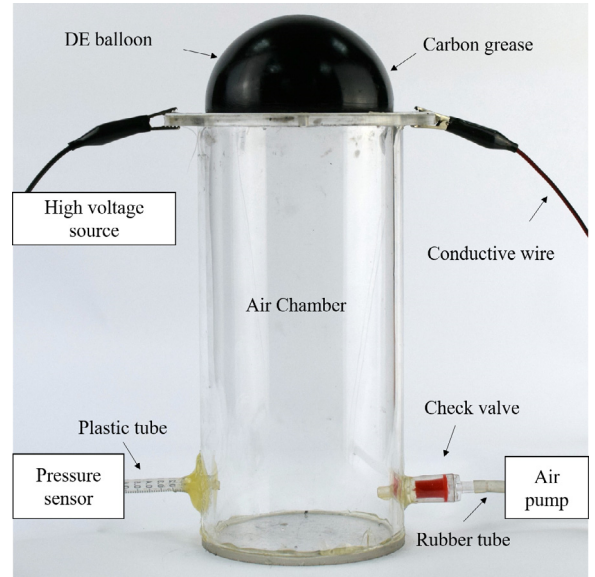

Fig. 1. Illustration of the experimental setup.

$\lambda_{\mathrm{pre}} = 1$, 200–850 Pa for $\lambda_{\mathrm{pre}} = 2$ and 500–800 Pa for $\lambda_{\mathrm{pre}} = 3$ with a step size of 50 Pa.

We consider first an initially un-stretched DE membrane, $\lambda_{\mathrm{pre}} = 1$, prior to inflation. Our experimental results in Fig. 2(a) show that for the tested initial inflation pressure range, the critical voltage for the nucleation of wrinkles, ϕ_c, increases with increasing initial inflation pressure, P_0. For the initial inflation pressure, $100 \leq P_0 \leq 300$ Pa, wrinkles nucleate first near the clamped edge of the DE balloon and then move out in the latitudinal direction as the applied voltage increases, albeit with larger longitudinal wavelengths. These results are different from the experimental results presented in Mao et al. [10] for $\lambda_{\mathrm{pre}} = 2$, where wrinkles nucleate near the apex of the DE balloon when initial inflation pressure is small, e.g., $P_0 = 500$ Pa. As P_0 increases, wrinkles nucleate near the mid-latitude or the clamped edge of the DE balloon depending on the magnitude of P_0 [10]. Moreover, results show that for $\lambda_{\mathrm{pre}} = 1$, $P_0 = 400$ Pa and $\phi = 5.5$ kV wrinkles appear simultaneously near the apex and the clamped edge of the DE balloon, while the mid-latitude is still flat. Furthermore, wrinkle-patterns change from stripe-like wrinkles near the edge of the DE balloon to labyrinth-like wrinkles near the apex of the DE balloon as the step voltage increases. We also note that amplitudes of the wrinkles are more significant at lower P_0 for the same applied step voltage (Fig. 2(a)). The reason for this phenomenon is that the increase in the compressive Maxwell stress due to thinning upon inflation is more significant than the increase in the tensile stress caused by the inflation. In the next section, we show that the relation between the critical voltage and the initial inflation pressure is not monotonic.

Fig. 2(b) shows evolution of wrinkles for a period of step voltage. As the critical voltage is reached, electromechanical phase transition occurs leading to a coexistence of flat and wrinkle states, and then, upon removing the voltage, wrinkles disappear and the surface becomes flat again. Thus, wrinkle instability of the inflated DE membrane is
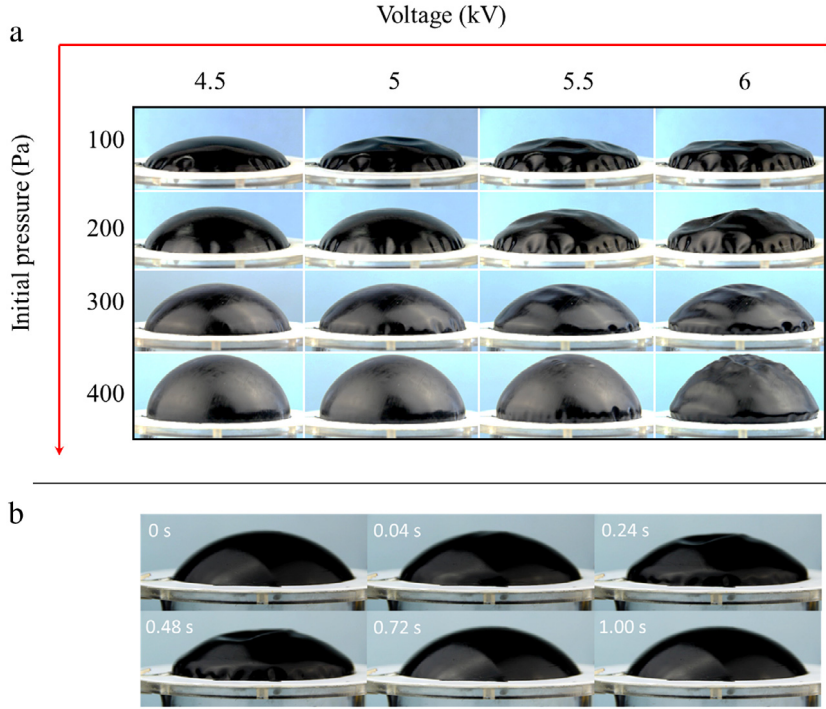
Fig. 2. Experimental analysis of DE balloon with pre-stretch $\lambda_{pre} = 1$. (a) Winkles of DE balloon subject to various applied voltages. The initial inflation pressure and applied voltage vary respectively from 100 Pa to 400 Pa and from 4.5 kV to 6 kV. (b) Wrinkles evolution of DE balloon in one period subject to applied voltage $\phi = 5$ kV (1 Hz) and initial inflation pressure $P_0 = 300$ Pa. A video showing the real-time transition between the flat and wrinkle states in (b) is provided in the supplementary material (Video S1, Appendix).

completely reversible. A video showing real-time transitions between wrinkle state and flat state during three-period of step voltage is provided in the supplementary material (Video S1, Appendix).

To examine the pre-stretch effect on wrinkle instability, we have conducted the experiment with $\lambda_{pre} = 2, 3, 4$. As shown in Fig. 3, for $\lambda_{pre} = 2, 3$ the position where wrinkles nucleate moves from the apex to the edge of the DE balloon as the initial inflation pressure increases. These observations are similar to the experimental observations reported in Mao et al. for DE membrane with $\lambda_{pre} = 2$ [10]. Experiments with $\lambda_{pre} = 4$ all failed with electrical breakdown near the edge before observing nucleation of wrinkles. The electrical breakdown of the DE balloon may be due to an artifact in the experimental setup, where the membrane is stretched non-uniformly before being clamped leading to excessive thinning near the clamped edge. A systematic discussion of the failure by electrical breakdown is given in Section 4.

3. Theoretical predictions of wrinkling conditions

Our experimental results show that pre-stretching the DE membrane affects wrinkle instability of the inflated DE balloon. In the following, analytical study is performed to shed some lights on the wrinkling of the DE membrane as a function of pre-stretch, initial inflation pressure and voltage. Following Mao et al. [10], the DE membrane is modeled using the membrane theory. Here for completeness, the key assumptions in deriving the

analytical model are stated as follows: (i) The shape change of the DE membrane during charging is assumed to be negligible; (ii) The total stress ($\mathbf{s}^+$) in the current configuration is the sum of the mechanical stress ($\mathbf{s}^-$) due to the mechanical loading and the compressive Maxwell stress ($-\mathbf{s}^M$) induced by the electric field; (iii) If either of the two in-plane stress components, s_i^+ ($i = 1, 2$) becomes negative, the membrane wrinkles immediately [11] and the wrinkle patterns depend on the stress state. If $s_2^+ < 0$ and $|s_1^+| < 0.5 |s_2^+|$, stripe-like wrinkles along the longitudinal direction nucleate. If $s_1^+ < 0$, $s_2^+ < 0$ and $|s_1^+| \geq 0.5 |s_2^+|$, labyrinth-like wrinkles emerge.

The boundary-value problem of an inflated clamped membrane is originally formulated by Adkins and Rivlin [12]. An equivalent derivation of the governing equations are presented in Mao et al. as follows [10],
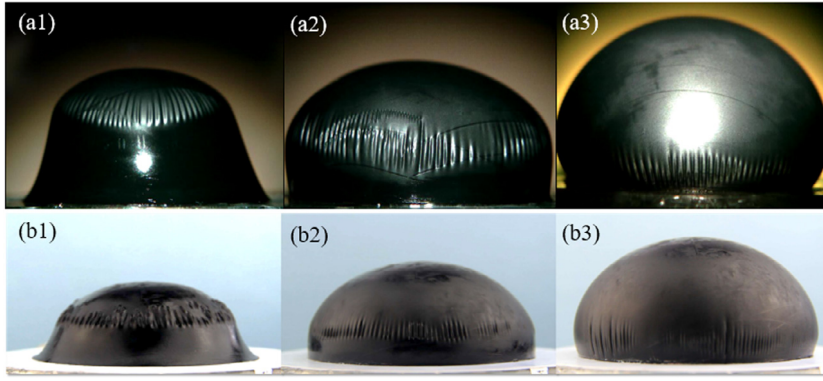
$$\frac{dr}{dR} = \lambda_1 \cos \theta \tag{1a}$$

$$\frac{dz}{dR} = -\lambda_1 \sin \theta \tag{1b}$$

$$\frac{d\theta}{dR} = -\frac{s_2^-}{s_1^-} \frac{\sin \theta}{R} + \frac{\lambda_1 \lambda_2}{s_1^-} \frac{P}{H_0} \tag{1c}$$

$$\frac{ds_1^-}{dR} = \frac{1}{R} \left(s_2^- \cos \theta - s_1^- \right) \tag{1d}$$

where λ_1 and λ_2 are the stretch ratios in the longitudinal and latitudinal directions, R and r are the radial positions of a material point in the un-deformed and deformed

Fig. 3. Wrinkles of DE balloon subject to various step voltages and initial inflation pressure. Subsets (a1–a3) and (b1–b3) correspond to DE membrane with $\lambda_{\mathrm{pre}} = 2$ and $\lambda_{\mathrm{pre}} = 3$ respectively. (a1) $\phi = 5$ kV, $P_0 = 700$ Pa, (a2) $\phi = 5$ kV, $P_0 = 800$ Pa, (a3) $\phi = 6$ kV, $P_0 = 850$ Pa, (b1) $\phi = 3.6$ kV, $P_0 = 500$ Pa, (b2) $\phi = 3.3$ kV, $P_0 = 700$ Pa and (b3) $\phi = 3.1$ kV, $P_0 = 800$ Pa.

configurations, respectively, z is the vertical position of the material point in the deformed configuration, and θ is the slope angle of the material point relative to the latitudinal direction.

The axisymmetric deformation of the inflated membrane requires the initial values at the apex of the DE balloon to be: $z(0) = 0$, $\theta(0) = 0$, $\lambda_1(0) = \lambda_{\mathrm{apx}}$, where λ_{apx} is the stretch at the center of the inflated DE membrane. The edge of the DE balloon is clamped which requires $r(R_0) = R_c$. Adopting Gent model [13] and DE field theory [14], the governing equations are solved numerically using the standard shooting method where Eq. (1d) is reformulated in terms of $d\lambda_1/dR$ (see the supplementary material for details, Appendix). For a given inflation pressure and pre-stretch ratio, the parameter λ_{apx} is varied until the clamped edge boundary condition $r(R_0) = R_c$ is satisfied.

In the following analysis, we adopt six dimensionless parameters,

$$\bar{R} = \frac{R}{R_0}, \qquad \bar{s}_1 = \frac{s_1}{\mu}, \qquad \bar{s}_2 = \frac{s_2}{\mu},$$

$$\bar{P}_0 = \frac{P_0}{\mu H_0/R_0}, \qquad \bar{\phi} = \frac{\phi}{H_0\sqrt{\mu/\varepsilon}}, \qquad \bar{V} = \frac{V}{R_0^3}$$

where μ is the shear modulus, ε is the permittivity of the DE, and V is the volume of the inflated DE membrane.

3.1. Critical voltage for wrinkling

Fig. 4(a) plots the critical voltage $\bar{\phi}_{c1}$ (solid lines) for which $\bar{s}_1^+ = 0$ and the critical voltage $\bar{\phi}_{c2}$ (dashed lines) for which $\bar{s}_2^+ = 0$, where λ_{pre} varies from 1 to 5. It shows that the relation between the critical voltage and the initial inflation pressure is not monotonic for low pressure with distinctly different behavior of the initially un-stretched membrane, $\lambda_{\mathrm{pre}} = 1$, versus the initially pre-stretched membrane, $\lambda_{\mathrm{pre}} = 2-5$. For the pre-stretched membrane, the critical voltages $\bar{\phi}_{c1}$ and $\bar{\phi}_{c2}$ are equal and decrease monotonically for $\bar{P}_0 < \bar{P}_{\mathrm{A-D}}$, respectively, beyond which they deviate significantly with $\bar{\phi}_{c2}$ always lower than $\bar{\phi}_{c1}$. However, for the un-stretched membrane $\lambda_{\mathrm{pre}} = 1$, there are three distinct regions: $\bar{\phi}_{c2} < \bar{\phi}_{c1}$ for $\bar{P}_0 < \bar{P}_{\mathrm{E}}$ and

$\bar{P}_0 > \bar{P}_{\mathrm{F}}$, and $\bar{\phi}_{c2} = \bar{\phi}_{c1}$ for $\bar{P}_{\mathrm{F}} < \bar{P}_0 < \bar{P}_{\mathrm{E}}$. These analytical calculations match with the experimental observations in Fig. 2(a), where most of the wrinkles for the un-stretched membrane are of stripe-like type.

To delineate the different trends of the $\bar{\phi}_c - \bar{P}_0$ curve near $\lambda_{\mathrm{pre}} = 1$, we computed $\bar{\phi}_{c1}$ and $\bar{\phi}_{c2}$ for $1.1 \leq \lambda_{\mathrm{pre}} \leq 1.4$. Fig. 4(b) reveals two critical pre-stretches $\lambda_{c1} = 1.26$ and $\lambda_{c2} = 1.12$ beyond which the relationship between $\bar{\phi}_{c1}, \bar{\phi}_{c2}$ and $\bar{P}_0$ show the same trend as in the case of $\lambda_{\mathrm{pre}} \geq 2$, respectively. Another critical pre-stretch $\lambda_{c3} = 1.33$ is detected beyond which the curves $\bar{\phi}_c - \bar{P}_0$ for $\bar{\phi}_{c1}$ and $\bar{\phi}_{c2}$ overlap when $\bar{P}_0$ is small similar to the cases with $\lambda_{\mathrm{pre}} \geq 2$ in Fig. 4(a).

In Fig. 5, the effect of the initial pre-stretch on the critical voltage $\bar{\phi}_{c2}$ is shown for various $\bar{P}_0$. It is noted that for a given $\bar{P}_0$, $\bar{\phi}_{c2}$ increases first with λ_{pre} then decreases. For each curve there is a critical λ_{pre} at which $\bar{\phi}_{c2}$ has a maximum that scales inversely proportional with $\bar{P}_0$. This behavior is an implication of the competition between the tensile stress due to the mechanical loading and the true compressive Maxwell stress defined as $s_1^M = s_2^M \propto \lambda_1\phi^2/h^2$, where ϕ is the applied voltage and h is the thickness of the DE membrane in the deformed state. The scaling of the Maxwell stress with h^{-2} was exploited in the experiment presented in Section 2 for the case with $\lambda_{\mathrm{pre}} = 1$. In this experiment, the DE membrane VHB 4905 ($h = 0.5$ mm) was replaced with the thinner DE membrane VHB 9473 ($h = 0.25$ mm) to reduce the critical voltage for wrinkling $\bar{\phi}_{c2}$ to below the maximum voltage (10 kV) generated by the step-voltage device. It is also noteworthy to indicate that for a large inflation pressure, $\bar{p}_0 > 1$, the DE membrane may have multiple critical voltages under the same mechanical loading. This is mainly because for certain values of $\bar{p}_0$, the balloon may have several stable equilibrium configurations with different volumes, e.g. $\bar{P}_0 = 1.8$ in Fig. 7.

3.2. Nucleation sites of wrinkles

Next, we determine the positions for nucleation sites of wrinkles, $\bar{R}_N$, as a function of $\bar{P}_0$ for various λ_{pre}. As shown in Fig. 6(a), for $\lambda_{\mathrm{pre}} = 2, 3, 4, 5$, the $\bar{R}_N - \bar{P}_0$
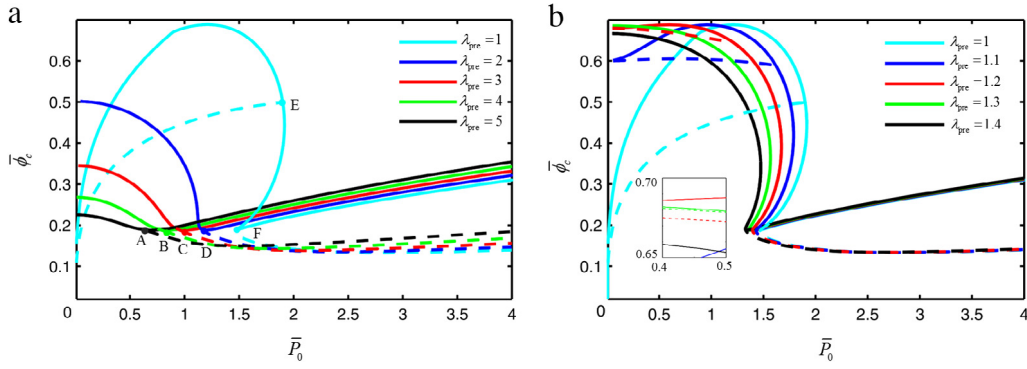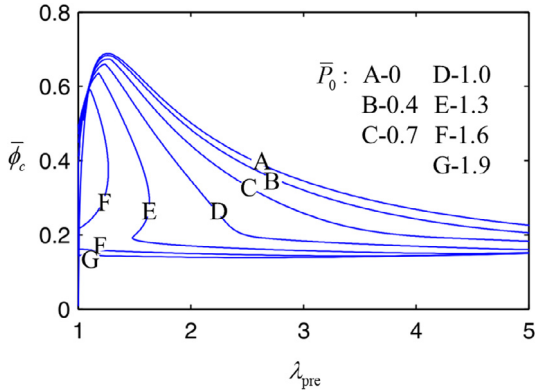
Fig. 4. Theoretical prediction of the critical voltage $\overline{\phi}_c$ vs. initial inflation pressure $\overline{P}_0$ for $\overline{s}_1^+ = 0$ (solid line) and $\overline{s}_2^+ = 0$ (dashed line) for different pre-stretches. (a) $\lambda_{\text{pre}} = 1, 2, 3, 4, 5$. Letters A–F denote the intersection of solid and dashed lines for each λ_{pre}. (b) $\lambda_{\text{pre}} = 1, 1.1, 1.2, 1.3, 1.4$. The inset shows details of $\overline{\phi}_c - \overline{P}_0$ curves within the range of $\overline{\phi}_c(0.65 - 0.7) - \overline{P}_0(0.4 - 0.5)$.
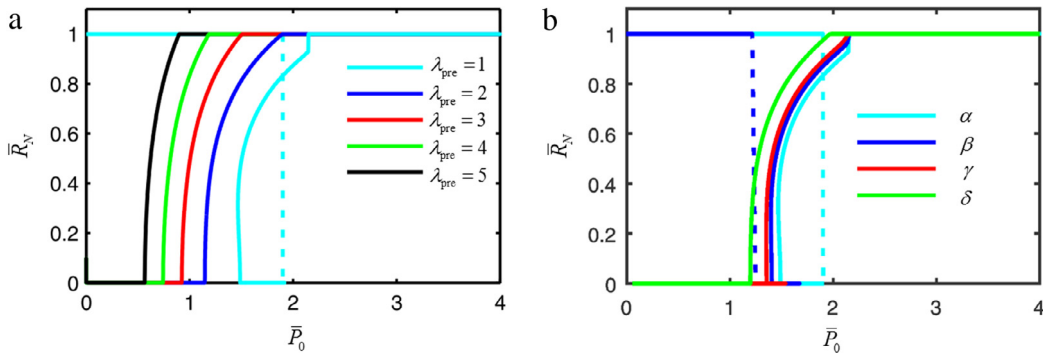
Fig. 6. Theoretical prediction of the radial position $\overline{R}_N$ where wrinkle nucleates under different initial inflation pressure $\overline{P}_0$ and different pre-stretches λ_{pre}. (a) $\overline{R}_N - \overline{P}_0$ curves with pre-stretches $\lambda_{\text{pre}} = 1, 2, 3, 4, 5$. (b) Four typical $\overline{R}_N - \overline{P}_0$ curves $\alpha, \beta, \gamma, \delta$ that correspond respectively to $\lambda_{\text{pre}} = 1$, $\lambda_{\text{pre}} = 1.2$, $\lambda_{\text{pre}} = 1.33$ and $\lambda_{\text{pre}} = 1.82$. (For interpretation of the references to color in this figure legend, the reader is referred to the web version of this article.)

**Fig. 5.** Theoretical prediction of critical voltage $\overline{\phi}_c$ as a function of pre-stretch ratio λ_{pre} for various initial inflation pressure $\overline{P}_0$, A–G: 0–1.9.

is monotonic with wrinkles nucleating at the apex for $\overline{P}_0 \leq 1.148, 0.925, 0.744, 0.568$, respectively, beyond which nucleation sites move monotonically along the latitudinal direction towards the clamped edge. In contrast, for $\lambda_{\text{pre}} = 1$, the $\overline{R}_N - \overline{P}_0$ curve is not monotonic with wrinkle nucleating at the apex for $\overline{P}_0 \leq 1.9$ and $\overline{P}_0 \geq 2.2$. Moreover, for $\overline{P}_0$ in the range between 1.49 and 1.9, wrinkle may nucleate simultaneously at the clamped edge,

the apex and somewhere along the latitudinal direction. We also note the steep slope of the curves $\overline{R}_N - \overline{P}_0$ near $\overline{P}_0 = 1.488$, and $\overline{P}_0 = 2.2$ which indicates that wrinkles may nucleate at a larger area for these pressure values. In Fig. 6(b), we delineate the different trends of the $\overline{R}_N - \overline{P}_0$ curves by plotting four curves α, β, γ and δ, that correspond respectively to $1 \leq \lambda_{\text{pre}} < 1.16$, $1.16 \leq \lambda_{\text{pre}} < 1.33$, $1.33 \leq \lambda_{\text{pre}} < 1.82$ and $\lambda_{\text{pre}} \geq 1.82$. These curves show that for slightly pre-stretched membrane, there is a pressure range at which wrinkle may nucleate instantaneously at several isolated sites, while for $\lambda_{\text{pre}} \geq 1.82$, $\overline{R}_N$ varies monotonically with $\overline{P}_0$ and wrinkles are expected to nucleate at a single site. These results are in agreement with the experimental observations in Figs. 2 and 3.

Fig. 7 shows $\overline{P}_0 - \overline{V}$ and $\overline{R}_N - \overline{V}$ curves for a DE balloon with $\lambda_{\text{pre}} = 1$. In contrast to $\overline{R}_N - \overline{P}_0$ curves, $\overline{R}_N - \overline{V}$ curves do not self-intersect providing non-ambiguous relation between the nucleation sites of wrinkles and volume of the inflated balloon. As shown in Fig. 7, wrinkles nucleate near the edge for $\overline{V} \leq 2.53$, after which nucleation sites jump suddenly towards the apex of the DE balloon as $\overline{V}$ increases beyond 2.53. For $\overline{V} > 20.10$, $\overline{R}_N$ increases monotonically with $\overline{V}$ and then transits steeply towards the edge at $\overline{V} = 174.69$. These results, show that for a volume controlled experiment, wrinkles nucleate in localized areas
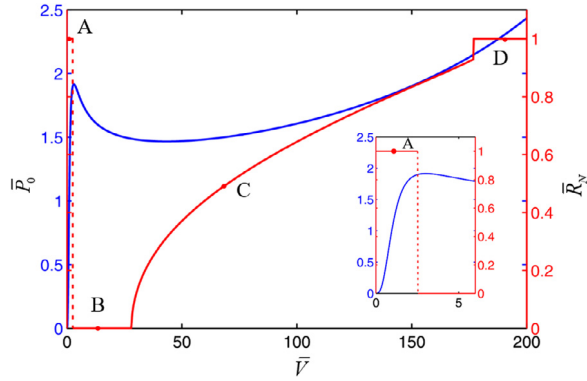
Fig. 7. Initial inflation pressure $\bar{P}_0$ versus volume of the DE balloon $\bar{V}$ (blue line) and position where wrinkles nucleate $\bar{R}_N$ versus volume of the DE balloon $\bar{V}$ (red line) for $\lambda_{\mathrm{pre}} = 1$. Four different states are noted as A ($\bar{P}_0 = 1$), B ($\bar{P}_0 = 1.53$), C ($\bar{P}_0 = 1.56$), D ($\bar{P}_0 = 2.2$). The inset shows the curves at small volumes. (For interpretation of the references to color in this figure legend, the reader is referred to the web version of this article.)

in contrast to results of the pressure controlled experiment shown in Fig. 6(a), where wrinkles may nucleate separately at different locations for $\lambda_{\mathrm{pre}} = 1$.

3.3. Three-dimensional phase diagram for DE membrane with $\lambda_{\mathrm{pre}} = 1$

In Fig. 8, we construct a three-dimensional phase diagram that represents the critical voltage and nucleation sites of wrinkles that correspond to points A, B, C and D in Fig. 7. For the 2D plane section that corresponds to A, stripe-like wrinkles nucleate at the clamped edge of the DE balloon for moderate voltage and throughout the surface for high applied voltage. This confirms the results in Fig. 2(a) for $P_0 = 100$ Pa where wrinkles are localized near the edge for $\phi = 4.5$ kV and spread throughout the whole surface for $\phi = 6$ kV. For the 2D plane section that corresponds to B, stripe-like wrinkles may appear near the edge while labyrinth-like wrinkles are expected to appear simultaneously near the apex of the DE membrane. Similar observations are reported in Fig. 2(a) for $P_0 = 400$ Pa and $\phi = 6$ kV. Simultaneous nucleation of wrinkles at two different sites is also predicted to occur for a section of the phase diagram between A and B. Sections that correspond to points C and D exhibit similar wrinkling behavior as the section that corresponds to point B.

4. Discussion and analysis of results

In the previous section, we have determined the critical voltage and nucleation sites for wrinkling instability. However, our experimental results showed that DE membrane may fail by electrical breakdown for $\lambda_{\mathrm{pre}} > 3$. The electrical breakdown strength of DE membrane has been investigated well both experimentally and theoretically [15,16]. According to Huang et al. [15], the electrical breakdown field E_B is related to the initial thickness H_0 and equal-biaxial stretch λ_{pre} as $E_B = 51 H_0^{-0.25} \lambda_{\mathrm{pre}}^{1.13}$. Here, we select the apex of the DE balloon which is the thinnest place and in an equal-biaxial stretch
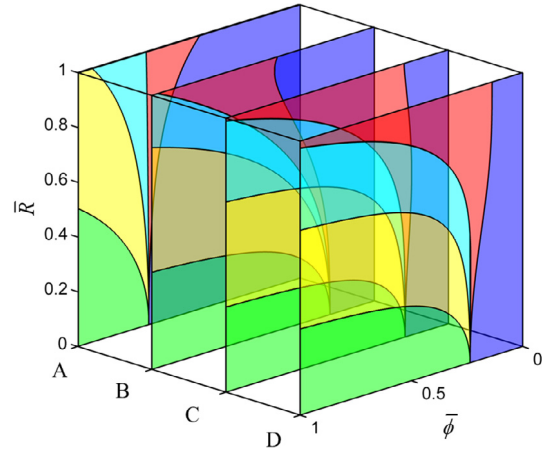

Fig. 8. 3D phase diagram of DE balloon with pre-stretch $\lambda_{\mathrm{pre}} = 1$ showing distribution of wrinkle-patterns along the longitudinal direction with four different initial states (A, B, C, D) before applying voltage. A, B, C and D are the same states as those in Fig. 7. The stress states are indicated by (i) blue, $\bar{s}_1^+ > 0$ and $\bar{s}_2^+ > 0$, (ii) red, $\bar{s}_1^+ > 0$ and $\bar{s}_2^+ \leq 0$, (iii) cyan, $|\bar{s}_1^+| < |0.5\bar{s}_2^+|$, $\bar{s}_1^+ \leq 0$, and $\bar{s}_2^+ \leq 0$, (iv) yellow, $|0.5\bar{s}_2^+| < |\bar{s}_1^+| \leq |0.9\bar{s}_2^+|$, $\bar{s}_1^+ \leq 0$, and $\bar{s}_2^+ \leq 0$, and (v) green, $|0.9\bar{s}_2^+| < |\bar{s}_1^+| \leq |\bar{s}_2^+|$, $\bar{s}_1^+ \leq 0$, and $\bar{s}_2^+ \leq 0$. (For interpretation of the references to color in this figure legend, the reader is referred to the web version of this article.)

to calculate the electrical breakdown field. Then, we substitute the stretch λ_{apex} at the apex of the DE balloon, to obtain $E_{\mathrm{Bapex}} = 51 H_0^{-0.25} \lambda_{\mathrm{apex}}^{1.13}$. The instant electrical field E_c at the apex of the DE balloon is calculated from the applied critical step voltage $\bar{\phi}_c$ on the DE balloon. In calculating the electrical breakdown field, we have adopted Gent material model with shear modulus $\mu = 50$ kPa and stretch limit $J_{\mathrm{lim}} = 220$ [17].

Our calculations show that $E_{\mathrm{Bapex}} < E_c$ and the DE balloon should not fail by electrical breakdown. Even we decrease the constant number of the electric field expression, the theoretical prediction cannot match the experimental observations of the repetitive breakdowns of the DE membrane with $\lambda_{\mathrm{pre}} > 3$. This discrepancy between the experimental results and the analytical predictions using the empirical expression proposed in Huang et al. [15] may be due to the excessive deformation near the clamped edge where electrical breakdown occurred in our experiment. Fig. S1 in the supplementary material show the theoretical estimate for the electrical breakdown near the apex and the clamped edge of DE membrane with $\lambda_{\mathrm{pre}} = 2$.

In Fig. 9, we draw the $\bar{P} - \bar{V}$ curves of DE balloon subject to $\lambda_{\mathrm{pre}} = 2$ and voltage $\bar{\phi}$ ranging from 0 to 0.4 with an interval equal to 0.1. Results show two types of $\bar{P} - \bar{V}$ curves: 1. Pressure increases monotonously with volume. 2. Pressure increases first and then drops down before increasing again as the volume increases. For the second type, we calculate the peak value at the apex of $\bar{P} - \bar{V}$ curves and obtain $\bar{\phi}_{\mathrm{apex}} - \bar{P}_{\mathrm{apex}}$ curves from a series of $\bar{P} - \bar{V}$ curves subjected to various voltages. When the pressure is larger than $\bar{P}_{\mathrm{apex}}$, the DE balloon may experience snap-through instability which induces the failure of DE balloon.

Comparing the $\bar{\phi}_{\mathrm{apex}} - \bar{P}_{\mathrm{apex}}$ curves and the $\bar{\phi}_c - \bar{P}_0$, we plot in Fig. 10 a phase diagram that demonstrates
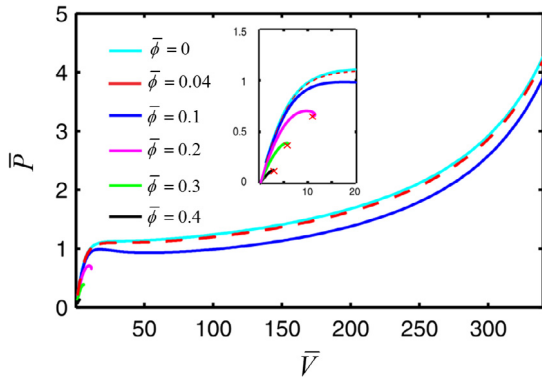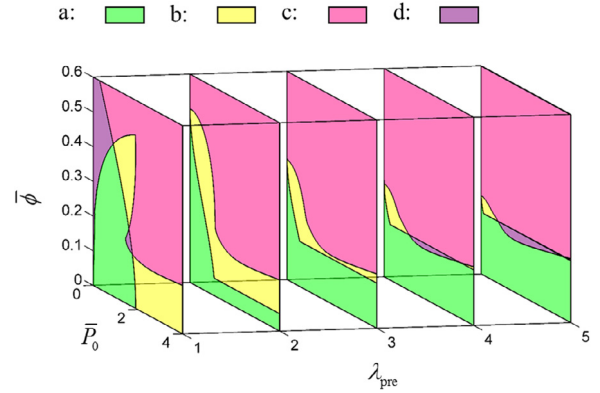
Fig. 9. $\overline{P} - \overline{V}$ curves for DE balloon in its equilibrium states with various voltages. The inset illustrates the $\overline{P} - \overline{V}$ curves at small volumes where the red × markers designate the critical points beyond which no equilibrium configurations are predicted by the present theory. (For interpretation of the references to color in this figure legend, the reader is referred to the web version of this article.)

Fig. 10. 3D phase diagram of DE balloon with $\lambda_{pre} = 1$ subject to electromechanical loads. (a) Safe area. (b) Snap-through may occur if the DE balloon is inflated within this area. (c) Wrinkles occur if the DE balloon is subject to a step voltage. (d) Cross area of (a) and (c). The pre-stretches are taken as $\lambda_{pre} = 1, 2, 3, 4, 5$.

the various states of the electromechanically activated DE membrane for different λ_{pre}. Flat state, wrinkle state, coexistent flat and wrinkle states and snap-through zones are marked in green, pink, purple, and yellow color respectively. For $\lambda_{pre} = 1$, there is a critical pressure $\overline{P}_0 \approx 2$ above which the DE membrane may experience snap-through instability for low applied step-voltage. However, as λ_{pre} increases beyond $\lambda_{pre} = 1$, the flat state zone spreads across $\overline{P}_0$ range, where snap-through zone separates the flat state zone and wrinkle state zone. Our experiments showed that once wrinkles nucleate, the membrane thins downs leading to electrical breakdown. However, as the voltage is removed, the membrane goes back to its flat state. Thus, by switching the step-voltage on/off, the surface morphology of the DE balloon may switch between flat state (green) and wrinkle state (pink) without experiencing snap-through instability. Finally, it is worth noting that wrinkle state and flat state may coexist at $\lambda_{pre} = 1$ or at $\lambda_{pre} \geq 4$.

5. Conclusion

In this study, experimental and theoretical analyses are conducted to study wrinkling of an inflated DE membrane. Our analyses show that pre-stretching the DE membrane plays a critical role in determining patterns and locations of wrinkles that may emerge once the critical voltage is reached. Our results show that critical conditions for wrinkle nucleation conditions and patterns can be modulated by controlling the pre-stretch λ_{pre}, initial inflation pressure $\overline{P}_0$ and step voltage ϕ. Our analytical model reveals the following:

- The initial nucleation sites of wrinkles can be modulated by controlling the initial pre-stretch of the DE membrane.
- For $\lambda_{pre} \leq 1.82$, wrinkles are more spread throughout the middle of the DE membrane for $1.5 \leq \overline{P}_0 \leq 2$ and may occur simultaneously at the apex and clamped edge of the DE membrane. The wrinkles are stripe-like at the edge of the DE balloon for lower initial inflation pressure.

- For $\lambda_{pre} \geq 1.82$, wrinkles are more localized near the apex for lower $\overline{P}_0$ with labyrinth-like patterns and near the clamped edge with stripe-like patterns for larger $\overline{P}_0$.
- The phase diagram in Fig. 10 shows that pre-stretching the DE membrane before inflation extends the range of the inflation pressure at which wrinkles can be controlled by switching the step voltage on/off without experiencing snap-through instability.

We also determine the critical conditions for snap-through instability and electrical breakdown. We find that once wrinkles nucleate, either snap-through instability and/or electrical breakdown always follow if the voltage is held. This explains why wrinkles were unstable in our experiments and always led to failure if applied voltage was not removed.

We finally note that our analytical model does not take into consideration the viscoelastic effect of the VHB membranes used in our experiment. However, it is expected that viscoelasticity may affect greatly the propagation of wrinkles and the failure of the DE membrane [18]. Moreover, in the experiments, we found that sinusoidal alternating voltage and slope voltage with proper frequency and amplitude can nucleate wrinkles which cannot be predicted by our theory. These important issues are currently under investigation and will be reported in a future paper.

Appendix A. Supplementary data

Supplementary material related to this article can be found online at http://dx.doi.org/10.1016/j.eml.2016.06.001.

References

[1] G. Mao, et al., Dielectric elastomer peristaltic pump module with finite deformation, Smart Mater. Struct. 24 (7) (2015) 075026.

[2] J. Liu, et al., Enhanced compressive sensing of dielectric elastomer sensor using a novel structure, J. Appl. Mech. 82 (10) (2015) 101004.

[3] I.A. Anderson, et al., A thin membrane artificial muscle rotary motor, Appl. Phys. A 98 (1) (2010) 75–83.

[4] L. Maffli, et al., Ultrafast all-polymer electrically tunable silicone lenses, Adv. Funct. Mater. 25 (11) (2015) 1656–1665.

[5] T. Li, S. Qu, W. Yang, Energy harvesting of dielectric elastomer generators concerning inhomogeneous fields and viscoelastic deformation, J. Appl. Phys. 112 (3) (2012) 034119.

[6] T. Li, et al., Giant voltage-induced deformation in dielectric elastomers near the verge of snap-through instability, J. Mech. Phys. Solids 61 (2) (2013) 611–628.

[7] S. Jin Adrian Koh, et al., Dielectric elastomer generators: How much energy can be converted? IEEE/ASME Trans. Mechatronics 16 (1) (2011) 33–41.

[8] Q. Wang, et al., Dynamic electrostatic lithography: Multiscale on-demand patterning on large-area curved surfaces, Adv. Mater. 24 (15) (2012) 1947–1951.

[9] P. Shivapooja, et al., Dynamic surface deformation of silicone elastomers for management of marine biofouling: laboratory and field studies using pneumatic actuation, Biofouling 31 (3) (2015) 265–274.

[10] G. Mao, et al., Nucleation and propagation of voltage-driven wrinkles in an inflated dielectric elastomer balloon, Soft Matter 11 (2015) 6569–6575.

[11] D.G. Roddeman, et al., The wrinkling of thin membranes: Part I—theory, J. Appl. Mech. 54 (4) (1987) 884–887.

[12] J.E. Adkins, R.S. Rivlin, Large elastic deformations of isotropic materials. IX. The deformation of thin shells, Philos. Trans. R. Soc. 244 (888) (1952) 505–531.

[13] A.N. Gent, A new constitutive relation for rubber, Rubber Chem. Technol. 69 (1) (1996) 59–61.

[14] Z. Suo, Theory of dielectric elastomers, Acta Mech. Solida Sin. 23 (6) (2010) 549–578.

[15] J. Huang, et al., The thickness and stretch dependence of the electrical breakdown strength of an acrylic dielectric elastomer, Appl. Phys. Lett. 101 (12) (2012) 122905.

[16] G. Kofod, et al., Actuation response of polyacrylate dielectric elastomers, J. Intell. Mater. Syst. Struct. 14 (12) (2003) 787–793.

[17] J. Zhu, et al., Two types of transitions to wrinkles in dielectric elastomers, Soft Matter 8 (34) (2012) 8840–8846.

[18] M. Kollosche, et al., Temporal evolution and instability in a viscoelastic dielectric elastomer, J. Mech. Phys. Solids 76 (2015) 47–64.